Marine Ice Sheet Collapse Potentially Under Way for the Thwaites Glacier Basin, West Antarctica

Ian Joughin *et al.*

Science **344**, 735 (2014);
DOI: 10.1126/science.1249055

27.3 mg of ODA HDCN in 10 ml of 0.5 M H_2SO_4, pH = 0); PHTs were insensitive to weak acids, neutral water, and basic conditions (table S4).

The exceptional Young's modulus of aromatic PHTs, combined with the observed reversibility of the reaction in strongly acidic conditions, makes the PHTs an unprecedented new class of thermosets, as most high-modulus materials are completely chemically inert and often very difficult, if not impossible, to rework or recycle. Given their high stability toward organic solvents, ODA PHTs could be used in environments where robust, solvent-resistant materials are necessary; moreover, they resist catastrophic failure associated with environmental stress cracking (fig. S27). The acid-promoted reversibility of ODA PHTs would allow them to become the first thermosets that are easily repolymerized or recycled. The ability to depolymerize the fully cured PHTs opens numerous applications such as reworkable encapsulates (*16*), which have been explored extensively for recovery of high-value components such as in microelectronics, although approaches commonly sacrifice the mechanical properties of the resin. This rework can lead to substantial cost savings, as often in high-value applications, thermoset components with a single defect can result in the entire part being scrapped because the intractability of traditional thermosets prevents their removal to effect repairs.

PEG oligomers (**4.2**) were also studied for their reactivity with paraformaldehyde. Although PEG PHTs were not formed at high temperature, PEG HDCNs (**4.3**) that formed at low temperature exhibited properties that were markedly different from those of the high-modulus ODA HDCNs and PHTs. HDCNs based on oligomeric PEG diamines formed elastic organogels with a melting temperature (T_m) of ~49°C by DSC, that completely reverted back to their original starting components in neutral water, which makes them promising candidates for reversible covalent constructs for a wide variety of applications that require reversible assemblies such as materials for cargo delivery. In addition to reversibility, PEG HDCN organogels exhibited self-healing properties; images and a video of its self-healing ability can be found in the supplementary materials (movie S1 and fig. S23). Previously reported polymerizations attempting to form PHTs focused on low-temperature reactions (50° to ~100°C) and used soluble aliphatic diamine monomers, or targeted PHTs, as reactive intermediates (*17*). These intermediate aliphatic diamine-based homopolymers were not extensively considered as useful thermosets because they exhibited poor mechanical properties (*18*). We believe, given the high rate of the reaction to its gelling point (within minutes) and difficulties we encountered to spectroscopically characterize ODA PHTs and HDCNs, that at these lower temperatures, low cross-link density, low-modulus HDCNs were most likely formed.

References and Notes

1. T. F. De Greef *et al.*, *Chem. Rev.* **109**, 5687–5754 (2009).
2. A. K. Singh, S. K. Shukla, M. A. Quraishi, *J. Mater. Environ. Sci.* **2**, 403–406 (2011).
3. M. Ghandi, F. Salimi, A. Olyaei, *Molecules* **11**, 556–563 (2006).
4. H. Ulrich, J. Rubinfeld, *J. Org. Chem.* **26**, 1637–1638 (1961).
5. J. Barluenga *et al.*, *J. Chem. Soc. Perkin Trans. 1* **1988**, 1631–1636 (1988).
6. A. Dandia, K. Arya, M. Sati, P. Sarawgi, *J. Fluor. Chem.* **125**, 1273–1277 (2004).
7. Z. Brunovska, J. P. Liu, H. Ishida, *Macromol. Chem. Phys.* **200**, 1745–1752 (1999).
8. A. G. Giumanini, G. Verardo, L. Randaccio, N. Bresciani-Pahor, P. Traldi, *J. Prakt. Chem.* **327**, 739–748 (1985).
9. E. A. Ponzio, R. Echevarria, G. M. Morales, C. Barbero, *Polym. Int.* **50**, 1180–1185 (2001).
10. A. D. Becke, *J. Chem. Phys.* **98**, 5648–5652 (1993).
11. M. W. Schmidt *et al.*, *J. Comput. Chem.* **14**, 1347–1363 (1993).
12. C. Lee, W. Yang, R. G. Parr, *Phys. Rev. B* **37**, 785–789 (1988).
13. V. Barone, M. Cossi, *J. Phys. Chem. A* **102**, 1995–2001 (1998).
14. K. R. Virwani, A. P. Malshe, W. F. Schmidt, D. K. Sood, *Smart Mater. Struct.* **12**, 1028–1032 (2003).
15. www.engineeringtoolbox.com/young-modulus-d_417.html; accessed 10 August 2013.
16. J.-S. Chen, C. K. Ober, M. D. Poliks, *Polymer (Guildf.)* **43**, 131–139 (2002).
17. A. Chermykh, J. Liu, H. Ishida, *Polymer (Guildf.)* **47**, 7664–7669 (2006).
18. M. Hiller, S. E. Evsyukov, *Mater. Res. Innov.* **6**, 179–184 (2002).
19. L. S. Schadler, S. C. Giannaris, P. M. Ajayan, *Appl. Phys. Lett.* **73**, 3842–3844 (1998).
20. S. Chou, H. C. Chen, H. E. Chen, *Compos. Sci. Technol.* **45**, 23–35 (1992).

Acknowledgments: This work was performed under a joint development agreement between IBM Research and King Abdulaziz City for Science and Technology (KACST) through the KACST-IBM Nanotechnology Center of Excellence (www.nce-kacst-IBM.org). Experimental procedures, NMR spectra, DFT Cartesian coordinates, x-ray diffraction data, nanoindentation data, and GPC traces can be found in the supplementary materials. We gratefully acknowledge J. Frommer for atomic force microscopy images, M. Sherwood for solid-state ^{13}C NMR experiments, T. Magbitang for thermal analysis, C. Fox for 4.6-kD PEG diamine synthesis, L. Randall for Instron data characterization, and R. King for assistance in nanoindentation measurements.

Supplementary Materials

www.sciencemag.org/content/344/6185/732/suppl/DC1
Materials and Methods
Figs. S1 to S30
Tables S1 to S4
References (*21–26*)
Movie S1

29 January 2014; accepted 2 April 2014
10.1126/science.1251484

Marine Ice Sheet Collapse Potentially Under Way for the Thwaites Glacier Basin, West Antarctica

Ian Joughin, Benjamin E. Smith, Brooke Medley

Resting atop a deep marine basin, the West Antarctic Ice Sheet has long been considered prone to instability. Using a numerical model, we investigated the sensitivity of Thwaites Glacier to ocean melt and whether its unstable retreat is already under way. Our model reproduces observed losses when forced with ocean melt comparable to estimates. Simulated losses are moderate (<0.25 mm per year at sea level) over the 21st century but generally increase thereafter. Except possibly for the lowest-melt scenario, the simulations indicate that early-stage collapse has begun. Less certain is the time scale, with the onset of rapid (>1 mm per year of sea-level rise) collapse in the different simulations within the range of 200 to 900 years.

Glaciers along the Amundsen Coast of Antarctica are thinning (*1*, *2*), producing the majority of Antarctica's contribution to sea-level rise (*3*, *4*). Much of this thinning is probably a response to the increased presence of warm modified Circumpolar Deep Water (CDW) on the adjacent continental shelf (*5*, *6*), which is melting and thinning the floating ice shelves that buttress the ice sheet (*7–9*). Thinner ice shelves are less able to restrain flow from the interior, contributing to feedbacks that increase ice discharge to the ocean (*10–14*). Thwaites and Haynes Glaciers, which hereafter we refer to collectively as Thwaites Glacier, produce just under half (52 Gt/year in 2007) of the Amundsen Coast losses (105 Gt/year in 2007) (*3*, *4*, *15*, *16*), making it one of the largest contributors to sea-level change. This glacier and the immediately adjacent and rapidly thinning Pine Island Glacier (*2*, *3*) were identified as potentially unstable several decades ago (*17*).

The present Thwaites grounding line—the location where ice reaches the ocean and goes afloat—rests on a coastal sill ~600 m below sea level (bsl) (Fig. 1) (*18*). At ~60 to 80 km farther inland, this sill gives way to a deep (>1200 m bsl) marine basin, yielding the potential for marine ice-sheet instability (*13*, *17*, *19–21*). Ice discharge is nonlinearly proportional to grounding-line thickness. Hence the potential for instability exists where the ice-sheet bed lies below sea level and steepens toward the interior, so that an initial retreat into deeper water creates a feedback,

Polar Science Center, Applied Physics Lab, University of Washington, 1013 NE 40th Street, Seattle, WA 98105–6698, USA.

leading to more thinning and retreat. Thus, with ongoing thinning and only tens of kilometers separating the grounding line from the marine basin's deepest regions, collapse of Thwaites Glacier may have already begun, albeit for now at a relatively moderate rate. To explore this possibility, we used a basin-scale ice-flow model to evaluate whether collapse is under way or if instead retreat may be limited by stabilizing factors.

We simulated Thwaites Glacier's response to subshelf melt using a prognostic, finite-element, depth-averaged, shallow-shelf model (*12*, *22*, *23*). We initialized the model by determining the basal shear stress and the ice-shelf rheological parameters that best matched the circa 1996 (1994–1996) observed velocity (*12*, *24*) and grounding line (*25*). At the ice/ocean interface, we used a simple depth-parameterized melt function scaled by a coefficient, m. With $m = 1$, this function produced steady-state behavior for neighboring Pine Island Glacier (*12*). For the Thwaites Ice Shelf, maximum melt rates with $m = 1$ are just over 200 m/year in the deepest regions, and total melt is 32 Gt/year when the simulation commences, making it comparable to a 1992–1996 steady-state estimate of 31 Gt/year for the shelf's highest-melt area (*26*).

Because the Amundsen Coast thinning appears to be driven by increased ice-shelf melting (*10*, *11*), many of our experiments are designed to examine this sensitivity to melt. First we examined the direct influence of melt on grounding-line position, with no feedback or response from the glacier, by fixing the velocity at its initial value throughout the simulation. These experiments reveal that grounding-line position is relatively insensitive to the direct effect of melting (*14*, *19*), producing nearly the same pattern of retreat for $m = 1$ and 4 (Fig. 2, A and B). The retreat that does occur is largely driven by the non–steady-state fixed velocity imposed at the start of the simulation.

Next we evaluated the model's response to melt (m = 0.5 to 4) with coupling (i.e., freely evolving velocity) to the ice sheet (Fig. 2, C to E). For these cases, there is a much greater sensitivity to melt, with the grounding line approaching the deepest parts of the trough for the higher-melt simulations (Fig. 2E). Strong melt (m = 2 to 4) produces ice loss at rates of <0.25 mm/year of sea-level equivalent (sle) for the first century, beyond which there is a period in each strong-melt simulation when the grounding line retreats abruptly, producing greater ice loss (0.25 to 0.5 mm/year of sle). Except for a few decades in the $m = 1$ simulation, ice loss for the lower melt simulations (m = 0.5 and 1) was less than observed in 2010 (Fig. 3A).

Antarctic accumulation rates are projected to increase over the 21st century (*27*). To evaluate any stabilizing effect such a change might have, we simulated a 20% linear increase in accumulation rate over the first 100 years, with a fixed rate thereafter (Fig. 3B). The higher accumulation moves the low-melt (m = 0.5 to 1)

?

shallow shelf…?

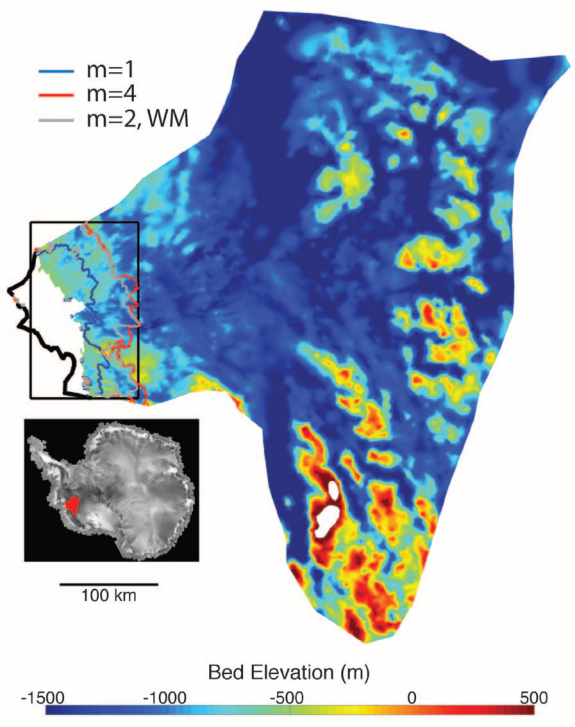

Fig. 1. Thwaites Glacier bed topography. Subglacial elevations were derived from airborne radar data (*23*). The heavy black line indicates the ice-shelf front, and the box indicates the area shown in Fig. 2. Blue, red, and gray lines indicate the grounding-line position at 250 years for the cases [$m = 1$, $m = 4$, and $m = 2$ with weak margins (WM)] shown in Fig. 2, D to F, respectively.

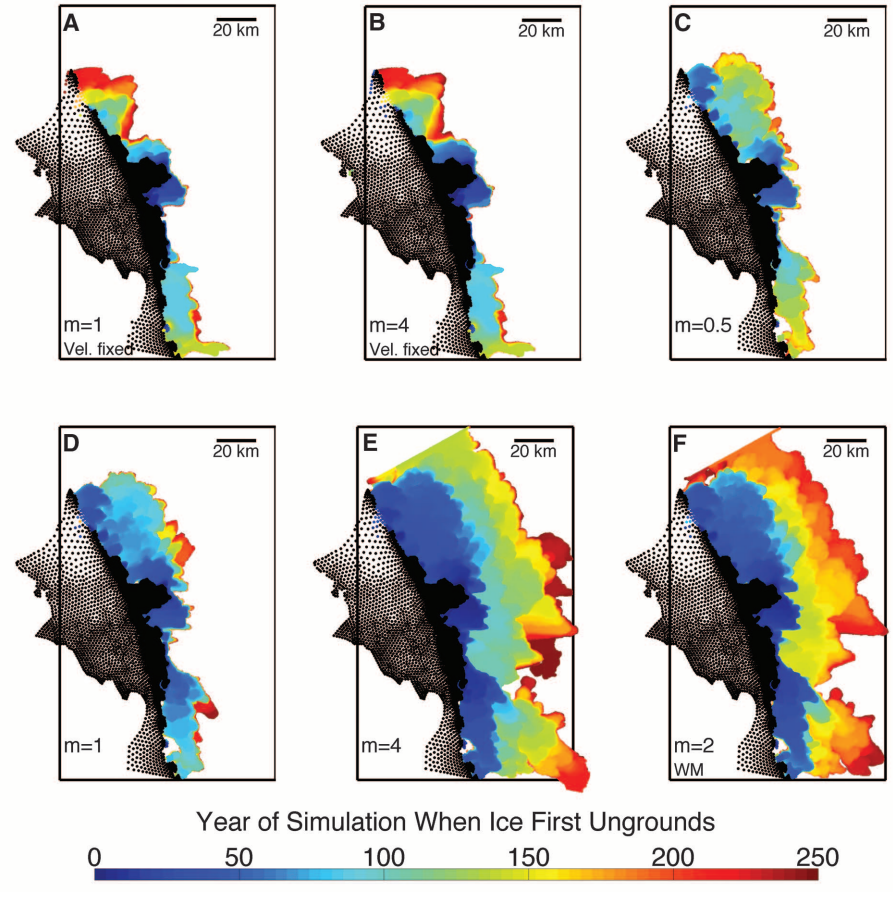

Fig. 2. Simulated ground line retreat for Thwaites Glacier. Time of ungrounding for simulations with fixed velocity for (**A**) $m = 1$ and (**B**) $m = 4$. The ungrounding time for freely evolving velocity with (**C**) $m = 0.5$, (**D**) $m = 1$, and (**E**) $m = 4$ is also shown. (**F**) Simulation with $m = 2$ for a shelf with weak margins. Black dots indicate ice-shelf nodes at the beginning of the simulation.

Table 1. Year in simulation when losses first exceed 1 mm/year of sle for standard and weak-margin models.

m	Standard model (year)	Weak-margin model (years)
0.5	>1000	>1000
1.0	870	573
2.0	460	342
3.0	343	253
4.0	292	212

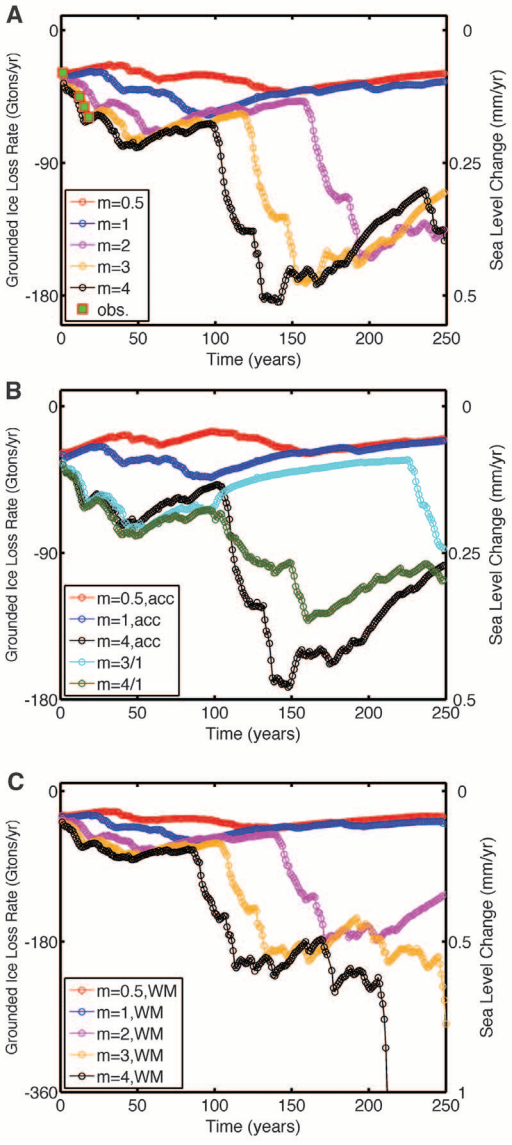

Fig. 3. Simulated ice losses for Thwaites Glacier. Annual rates of grounded ice loss (i.e., ice above flotation) for (**A**) initial model runs with $m = 0.5$ to 4. Green squares with red borders show observed losses for 1996 (1994–1996), 2007, 2010, and 2013 plotted as years 1, 12, 15, and 18, respectively (*15*, *16*). (**B**) Losses for experiments with a linear increase in accumulation by 20% over the first 100 years (acc) and high-melt cases for only the first 100 years (3/1 and 4/1). (**C**) Model runs with weakened ice-shelf margins for $m = 0.5$ to 4.

simulations closer to balance. For the higher-melt case ($m = 4$), it delays the transition to large losses (>90 Gt/year) by just under a decade.

Currently, elevated melt rates on the Amundsen Coast are largely driven by increased transport of warm CDW onto the continental shelf rather than by direct warming of the CDW (*6*). If the conditions responsible for this transport abate, melting should lessen. Thus, we simulated 100 years of high melt ($m = 3$ and 4) followed by reduced melt ($m = 1$) for the remainder of the simulation (Fig. 3B). Although the reduction in melt slowed the rate of loss, at the end of these 250-year simulations, losses were substantially greater relative to the sustained $m = 1$ simulation.

Inversions for the strength of ice-shelf shear margins often reveal substantial weakening due to either rheological softening (e.g., fabric or strain heating) (*28*) or mechanical damage (e.g., crevassing or rifting) (*29*). Our model includes weaker margins on the initial ice shelf, but as the shelf expands into the originally grounded ice, the newly formed ice-shelf margins remain strong. To evaluate the sensitivity to margin weakening, we implemented an ad hoc weakening scheme (*23*) and repeated our standard set of experiments. For the $m = 3$ simulation, weakening of the margins produces more extensive grounding-line retreat (Fig. 2F). For the highest-melt case ($m = 4$), at about 212 years into the simulation (Table 1), the grounding line recedes rapidly to the basin's deepest regions, yielding a sea-level contribution of more than 1 mm/year.

When simulated losses exceed 1 mm/year of sle, much greater losses generally follow within a few years. Using our basin-scale model, however, such rapid collapse is difficult to model, especially because interaction with other basins becomes increasingly important. Thus, we take 1 mm/year of sle to be a threshold that, once crossed, marks the onset of rapid (decades) collapse as the grounding line reaches the deepest regions of the marine basin. In our 250-year simulations, only the highest-melt, weak-margin simulation reaches this critical threshold. Therefore, we have extended the remaining simulations to determine when this threshold is reached (fig. S2 and Table 1). For all but the lowest-melt simulations ($m = 0.5$), the onset of rapid collapse begins within a millennium.

The observed losses from 1996 to 2013 (Fig. 3A) fall between the results from our highest-melt ($m = 3$ and 4) simulations. Over this period, the average simulated melt of 84 Gt/year for $m = 4$ agrees well with recent melt estimates of 69 to 97 Gt/year (*7*, *8*), indicating that the higher-melt simulations' early stages reasonably approximate present conditions. Thus, the close agreement between model and observation strengthens the argument that recent losses are melt-driven (*10*). Specifically, melt-induced ice-shelf thinning reduces buttressing, causing an initial speedup. In turn, this initial speedup causes the grounding line to retreat, resulting in loss of traction and far greater speedup and retreat. The ice stream was already out of balance before 1996, which may have been the result of thinning that caused the ice to unground several decades or more ago from a ridge seaward of the present grounding line (*3*, *30*).

Our simulations are not coupled to a global climate model to provide forcing nor do they include an ice-shelf cavity-circulation model to derive melt rates. Few if any such fully coupled models presently exist (*13*). As such, our simulations do not constitute a projection of future sea level in response to projected climate forcing. The results, however, indicate the type of behavior that is likely to occur. In particular, all the simulations show the grounding line stepping back in stages with concurrent increases in discharge, consistent with other models and observations of paleo–ice-stream retreat (*31*, *32*). The intensity of melt in our simulations regulates the time scale over which this pattern of retreat

occurs. Thus, although cavity-circulation models driven by regional ocean circulation models coupled to global climate models might yield differing spatiotemporal variations in melt, they should produce patterns of retreat similar to those we have simulated, but with tighter constraints on the timing.

An important feature of our numerical simulations is that they reveal a strong sensitivity to mechanical and/or rheological weakening of the margins, which can accelerate the rate of collapse by decades to centuries. Thus, future models will require careful treatment of shear margins to accurately project sea-level rise. Our simulations also assume that there is no retreat of the ice-shelf front. Full or partial ice-shelf collapse should produce more rapid retreat than we have simulated. In addition, we have not modeled ocean-driven melt that extends immediately upstream of the grounding line, which could also accelerate retreat (*32*).

Our simulations provide strong evidence that the process of marine ice-sheet destabilization is already under way on Thwaites Glacier, largely in response to high subshelf melt rates. Although losses are likely to be relatively modest over the next century (<0.25 mm/year of sle), rapid collapse (>1 mm/year of sle) will ensue once the grounding line reaches the basin's deeper regions, which could occur within centuries. Such rapid collapse would probably spill over to adjacent catchments, undermining much of West Antarctica (*18*). Similar behavior also may be under way on neighboring Pine Island Glacier (*12*, *33*). Unless CDW recedes sufficiently to reduce melt well below present levels, it is difficult to foresee a stabilization of the Thwaites system, even with plausible increases in surface accumulation. Although our simple melt parameterization suggests that a full-scale collapse of this sector may be inevitable, it leaves large uncertainty in the timing. Thus, ice-sheet models fully coupled to ocean/climate models are required to reduce the uncertainty in the chronology of a collapse. Nonetheless, the similarity between our highest melt rates and present observations suggests that collapse may be closer to a few centuries than to a millennium.

References and Notes

1. H. D. Pritchard, R. J. Arthern, D. G. Vaughan, L. A. Edwards, *Nature* **461**, 971–975 (2009).
2. A. Shepherd, *Geophys. Res. Lett.* **29**, 1364 (2002).
3. E. Rignot, *Geophys. Res. Lett.* **35**, L12505 (2008).
4. A. Shepherd *et al.*, *Science* **338**, 1183–1189 (2012).
5. S. S. Jacobs, A. Jenkins, C. F. Giulivi, P. Dutrieux, *Nat. Geosci.* **4**, 519–523 (2011).
6. M. Thoma, A. Jenkins, D. Holland, S. Jacobs, *Geophys. Res. Lett.* **35**, L18602 (2008).
7. E. Rignot, S. S. Jacobs, J. Mouginot, B. Scheuchl, *Science* **341**, 266–270 (2013).
8. M. A. Depoorter *et al.*, *Nature* **502**, 89–92 (2013).
9. H. D. Pritchard *et al.*, *Nature* **484**, 502–505 (2012).
10. A. Shepherd, D. Wingham, E. Rignot, *Geophys. Res. Lett.* **31**, L23402 (2004).
11. A. Payne, A. Vieli, A. Shepherd, D. Wingham, E. Rignot, *Geophys. Res. Lett.* **31**, L23401 (2004).
12. I. Joughin, B. E. Smith, D. M. Holland, *Geophys. Res. Lett.* **37**, L20502 (2010).
13. I. Joughin, R. B. Alley, D. M. Holland, *Science* **338**, 1172–1176 (2012).
14. O. Gagliardini, G. Durand, T. Zwinger, R. C. A. Hindmarsh, E. Le Meur, *Geophys. Res. Lett.* **37**, L14501 (2010).
15. B. Medley *et al.*, *Cryosphere Discuss.* **8**, 953–998 (2014).
16. J. Mouginot, E. Rignot, B. Scheuchl, *Geophys. Res. Lett.* **41**, 1576–1584 (2014).
17. T. J. Hughes, *J. Glaciol.* **27**, 518–525 (1981).
18. J. Holt *et al.*, *Geophys. Res. Lett.* **33**, L09502 (2006).
19. C. Schoof, *J. Geophys. Res. Earth Surf.* **112**, F03S28 (2007).
20. J. Weertman, *J. Glaciol.* **13**, 3–11 (1974).
21. J. H. Mercer, *Nature* **271**, 321–325 (1978).
22. D. R. MacAyeal, *J. Geophys. Res. Solid Earth* **94**, 4071–4087 (1989).
23. Model details are provided in the supplementary materials.
24. I. Joughin *et al.*, *J. Glaciol.* **55**, 245–257 (2009).
25. E. Rignot, J. Mouginot, B. Scheuchl, *Geophys. Res. Lett.* **38**, L10504 (2011).
26. E. Rignot, S. S. Jacobs, *Science* **296**, 2020–2023 (2002).
27. C. Genthon, G. Krinner, H. Castebrunet, *Ann. Glaciol.* **50**, 55–60 (2009).
28. E. Larour, E. Rignot, I. Joughin, D. Aubry, *Geophys. Res. Lett.* **32**, L05503 (2005).
29. C. P. Borstad, E. Rignot, J. Mouginot, M. P. Schodlok, *Cryosphere Discuss.* **7**, 3567–3610 (2013).
30. K. J. Tinto, R. E. Bell, *Geophys. Res. Lett.* **38**, L20503 (2011).
31. S. S. R. Jamieson *et al.*, *Nat. Geosci.* **5**, 799–802 (2012).
32. B. R. Parizek *et al.*, *J. Geophys. Res.* **118**, 638–655 (2013).
33. L. Favier *et al.*, *Nat. Clim. Change* **4**, 117–121 (2014).

Acknowledgments: Comments by M. Maki, D. Shapero, and four anonymous reviewers improved the manuscript. NSF supported I.J. and B.M.'s contribution (grants ANT-0424589 and ANT-0631973), and B.E.S. was supported by NASA (grant NNX09AE47G). We acknowledge NASA's Operation IceBridge, which provided much of the data used to constrain the model. The data used to constrain the model are archived at the University of Washington Library (http://dx.doi.org/10.6069/H5CC0XMK).

Supplementary Materials

www.sciencemag.org/content/344/6185/735/suppl/DC1
Materials and Methods
Supplementary Text
Figs. S1 and S2
References (*34*–*37*)

27 November 2013; accepted 21 April 2014
10.1126/science.1249055

Stick Insect Genomes Reveal Natural Selection's Role in Parallel Speciation

Víctor Soria-Carrasco,[1]* Zachariah Gompert,[2]* Aaron A. Comeault,[1] Timothy E. Farkas,[1] Thomas L. Parchman,[3] J. Spencer Johnston,[4] C. Alex Buerkle,[5] Jeffrey L. Feder,[6] Jens Bast,[7] Tanja Schwander,[8] Scott P. Egan,[9] Bernard J. Crespi,[10] Patrik Nosil[1]†

Natural selection can drive the repeated evolution of reproductive isolation, but the genomic basis of parallel speciation remains poorly understood. We analyzed whole-genome divergence between replicate pairs of stick insect populations that are adapted to different host plants and undergoing parallel speciation. We found thousands of modest-sized genomic regions of accentuated divergence between populations, most of which are unique to individual population pairs. We also detected parallel genomic divergence across population pairs involving an excess of coding genes with specific molecular functions. Regions of parallel genomic divergence in nature exhibited exceptional allele frequency changes between hosts in a field transplant experiment. The results advance understanding of biological diversification by providing convergent observational and experimental evidence for selection's role in driving repeatable genomic divergence.

Whether evolution is predictable and repeatable is difficult to test yet central to our understanding of biological diversification (*1*–*6*). Instances of repeated, parallel evolution in response to similar environmental pressures provide evidence of evolution by natural selection and can involve repeated divergence at specific genes (*7*–*9*). Indeed, parallel evolution of individual phenotypic traits has been estimated to involve the same genomic regions 30 to 50% of the time (*8*). Parallel evolution can also result in replicate species formation (i.e., parallel speciation) (*10*), but the genome-wide consequences of this process are unclear (*7*, *8*, *11*). Although some genomic regions will likely diverge repeatedly during parallel speciation, many might show idiosyncratic patterns because of contingencies such as the order in which mutations arise (*7*, *8*, *10*, *11*).

Even if repeated divergence occurs for some genomic regions (*7*, *12*, *13*), the underlying causes of this parallelism often remain speculative because it is difficult to disentangle the

[1]Department of Animal and Plant Sciences, University of Sheffield, Sheffield S10 2TN, UK. [2]Department of Biology, Utah State University, Logan, UT 84322, USA. [3]Deparment of Biology, University of Nevada, Reno, NV 89557, USA. [4]Department of Entomology, Texas A&M University, College Station, TX 77843, USA. [5]Department of Botany, University of Wyoming, Laramie, WY 82071, USA. [6]Department of Biology, Notre Dame University, South Bend, IN 46556, USA. [7]J. F. Blumenbach Institute of Zoology and Anthropology, University of Göttingen, 37073 Göttingen, Germany. [8]Department of Ecology and Evolution, University of Lausanne, Lausanne CH-1015, Switzerland. [9]Department of Ecology and Evolutionary Biology, Rice University, Houston, TX 77005, USA. [10]Department of Biological Sciences, Simon Fraser University, Burnaby, BC V5A 1S6, Canada.

*These authors contributed equally to this work.
†Corresponding author. E-mail: p.nosil@sheffield.ac.uk